J. Fluid Mech. (2001), *vol.* 444, *pp.* 299–320. Printed in the United Kingdom

Symmetry and the hydrodynamic blow-up problem

By RICHARD B. PELZ

Mechanical and Aerospace Engineering, Rutgers University, Piscataway, NJ 08854-8058, USA

(Received 4 April 2000 and in revised form 30 January 2001)

The problem of whether a spontaneous singularity can occur in finite time in an incompressible inviscid fluid flow is addressed. As suggested by previous numerical simulations, candidate flows are restricted to be invariant under the octahedral group of symmetries and to have a compact vortex tube in the fundamental domain. It is shown that in such a flow the image vorticity contributes strongly to the axial strain rate on the fundamental in a way which is only weakly proportional to the curvature of the vortex lines. Analysis of a model flow shows that axial strain rate scales as the inverse square of the distance to the origin, and that the velocity field forms a topological trap in which the vortex tube is accelerated towards the origin – a degenerate critical point. Evidence from simulations supports these findings. These features suggest that linear strain rate/vorticity coupling can occur in a finite-time pointwise collapse of such symmetric flows.

1. Introduction

Whether a spontaneous singularity in an incompressible flow may develop in a finite time is still an open question. More than just a mathematical problem of regularity, it has relevance to the theory of turbulence and cascade mechanisms as well as possible focusing applications.

The subtle task of differentiating between a flow in which a singularity actually sits on the real time axis versus one with a pair of singularities a short distance away in the complex plane is, however, virtually impossible in a computer solution of the initial-value problem. Numerical evidence usually comes from fitting a flow variable to some $(t_{crit} - t)^{-\gamma}$ behaviour, but the difference in behaviour of the functions $1/\tau$ and $1/\sqrt{\tau^2 + \epsilon^2}$ where $\tau = t_{crit} - t$ comes only when τ is on the order of ϵ. If this evidence is based on integration to a time T, $0 < T < t_{crit}$, then ϵ can be assumed to be less than $t_{crit} - T$ to counter any blow-up conjecture.

A number of such candidate blow-up solutions of the Euler and Navier–Stokes equations have, nevertheless, been proposed (Kerr 1993; Boratav & Pelz 1994; Grauer, Marliani & Germaschewski 1998). These candidates should not be discarded as suggested by the argument above, but should be used to motivate further analytic studies.

In this paper, flows with the high symmetry assumed in one candidate solution (Boratav & Pelz 1994) are analysed. In particular, the relation between vorticity and axial strain rate is examined for flows invariant under the action of a particular symmetry group. A simple vortex flow in this space is then constructed and analysed further. For flows having octahedral symmetry and having a coherent vortex tube

of mild curvature which intersects a plane of reflectional symmetry, it is found that

positive strain rate in the direction of the vorticity is produced by the image vorticity;
this strain rate remains positive as curvature goes to zero;
this strain rate increases as the inverse square of the distance to the origin; and
the image vorticity causes the fundamental vortex to accelerate towards the origin, a degenerate critical point.

Strain rate and velocity fields from the numerical simulations confirm these findings. The suggested behaviour is a localized self-similar collapse towards the origin ending in finite-time blow-up.

This is not a proof of the existence of blow-up solutions. Evidence in this paper, while being patterned after observations of numerical experiments, is from constructed models. It provides, however, an understanding of how in such flows a coupling between strain rate and vorticity could be created and sustained through an image/collapse scenario.

There is little doubt that flows with octahedral symmetry will be unstable to perturbations which break the symmetry. The relationship of this work to real flows and especially turbulent flows is thus quite weak. Other candidate flows, such as Kerr (1993), Grauer *et al.* (1998), assume fewer symmetries and hence are more realistic. It is not clear, however, how to analyse these flows other than data reduction from larger computations. In this paper we pursue analysis in the less realistic high-symmetry flows in hope of identifying and understanding one blow-up solution more completely.

Starting with existing theorems, the subject of finite-time singularities in incompressible flow is reviewed and the present study motivated. Beale, Kato & Majda (1984) showed that the time integral of $|\omega|_{max}$ must become infinite in order for a flow to lose regularity. From this, the standard scenario of $|\omega|_{max}$ becoming infinite as $1/(t_{crit} - t)$ is assumed. (Recently, Ohkitani & Gibbon (2000) have shown numerically, and Constantin (2000) and Malham (2000) analytically that a large class of infinite-energy, two-dimensional forced flows become singular in finite time.) Then, as Majda (1986) pointed out, if the vorticity is to blow up at a point, the eigenvector associated with a positive eigenvalue of the strain rate must be roughly aligned with the vorticity vector. From the vorticity equation, $\mathrm{d}\omega/\mathrm{d}t = S\omega$, it is seen that nonlinear growth occurs in this fashion. The wavelength of the singular region was linked to the frequency through energy conservation by Constantin (1994); an algebraic blow-up of vorticity must be accompanied by an algebraic decrease in length scale.

Phenomenologically, the picture is of a vortex tube being stretched by an axial strain rate. Since exponential growth occurs when the strain rate is constant, strain rate must also become singular in order for vorticity to follow (see Moffatt 2000). In fact, for ω to scale as $1/(t_{crit} - t)$, axial strain rate must be linearly proportional to vorticity. The one-way interaction of a vortex being stretched by neighbouring tubes will not have such a coupling. An alternative is a 'self-stretching' scenario, in which a vortex structure creates a strain-rate field about itself with proper direction and coupling characteristics making the strain rate a function of the local vorticity.

Constantin (1994) showed through the analysis of the strain rate as a singular integral operator of the vorticity, that for an isolated vortex tube to stretch itself, the curvature of vortex lines must become infinite, leading to the theorem that if the vorticity direction field remains coherent, there is no finite-time blow-up for finite velocity (Constantin, Fefferman & Majda 1996). The radius of curvature of a vortex

tube is the length that must go to zero for blow-up. In § 2 this singular integral operator is examined more closely.

Rather than an isolated tube, a collection of vortex tubes linked by symmetry may create self-stretching. Recall that the equations of motion are invariant under translations, reflections and rotations. That is, a symmetry that exists in a flow at one time will be preserved for all time after. The idea is to add enough viable symmetries to construct a flow in which the strain rate acting axially on the fundamental vorticity is produced by the image vorticity. Then, in this 'image/collapse' scenario, the problem of blow-up moves to one of sustaining this arrangement while the length between fundamental and image goes to zero.

Simulations of collapse of anti-parallel vortex tubes, one candidate for blow-up (Kerr 1993; Pumir & Siggia 1990; Shelley, Meiron & Orszag 1993), make use of reflectional symmetries. A symmetry plane parallel to a tube creates the anti-parallel image. This symmetry seems to be attracting since vortex tubes with random alignment tend to align in an anti-parallel fashion and collapse (Boratav, Pelz & Zabusky 1992). As pointed out by Constantin (1994), however, the same vortex-line curvature restriction as in the isolated tube exists here. In § 3, it will be shown that reflectional symmetries do not add new strain rate/vorticity coupling. Furthermore, it will be shown that curvature of vortex lines tends to decrease when axial strain rate is large.

In § 4, a rotational symmetry is added to the reflectional ones to create an octahedral symmetry. It is shown through analysis of the strain rate as an integral operator of vorticity, that there exists a new, robust, strain rate/vorticity coupling which is positive even when the curvature of the vortex tubes is zero, thus removing the curvature restriction for blow-up. The velocity field under such symmetries is shown to be highly restricted with a degenerate critical point at the origin. Using an approximate model the velocity field induced by the images will be shown to 'trap' vorticity in the symmetry plane and create an accelerating flow towards the origin.

In § 5, analysis of previous numerical simulations with octahedral symmetry is performed. In the Biot-Savart vortex filament model, a linear coupling between strain rate and local vorticity is demonstrated, and that this coupling exists up to a time close to the critical time. In the field computations, a significant coupling is shown to exist, but due to resolution limitations, the quantitative identification of the time scaling is not possible. In both cases, the vortex structure appears to implode to the origin in a locally self-similar manner.

Finally, § 6 contains a discussion on the ramifications of these results and directions for further analysis.

2. Singular integral operator

The vorticity equation for an inviscid flow in an unbounded domain can be written as the following integral:

$$\frac{\mathrm{d}}{\mathrm{d}t}\omega(\bar{x}) = \omega(\bar{x}) \quad PV \int \mathscr{D}(x-\bar{x})\omega(x)\,\mathrm{d}^3x \tag{2.1}$$

where the strain rate is an integral operator of vorticity. This operator is of the Calderon–Zygmund, classical strongly singular type (Neri 1970; Constantin 1994). Integration is over all $\mathscr{R}^3$ for a flow with compact vorticity and no boundaries. In three dimensions, the function $\mathscr{D}$ has homogeneity of degree-3 and is found through differentiation of the Biot-Savart law

$$S_{i,j}(\bar{x}) = \frac{3}{8\pi} PV \int [\epsilon_{jkl}(x_i - \bar{x}_i) + \epsilon_{ikl}(x_j - \bar{x}_j)](x_k - \bar{x}_k)\omega_l(x)\frac{\mathrm{d}^3x}{|x-\bar{x}|^5}. \tag{2.2}$$

A specific example of this integral is the strain rate, $S_{1,1} = u_{1,1}$, evaluated at the point $\bar{x} = (0, \bar{x}_2, \bar{x}_3)$

$$u_{1,1}(0, \bar{x}_2, \bar{x}_3) = \frac{3}{8\pi} PV \int \frac{x_1[(x_2 - \bar{x}_2)\omega_3(x) - (x_3 - \bar{x}_3)\omega_2(x)]}{[x_1^2 + (x_2 - \bar{x}_2)^2 + (x_3 - \bar{x}_3)^2]^{5/2}} \mathrm{d}^3x. \tag{2.3}$$

One can see from the above expression that this is the strain rate which is needed for nonlinear growth of ω_1 ($\mathrm{d}\omega_1/\mathrm{d}t = \omega_i u_{1,i}$) in the plane. The integrand, however, is a function of the other two components of vorticity, implying that the behaviour of the local curvature of vortex lines is critical for the production of axial strain rate. Indeed, if the flow is assumed to have reflectional symmetry about $x_1 = 0$, to first order the vorticity components near $x = \bar{x}$ are $\omega_i(x) = \kappa_i(\bar{x})\omega_1(\bar{x})x_1$ for $i = 2, 3$ and where κ_i is the curvature of vortex lines at $x = \bar{x}$. In order to keep zero homogeneity of the singular integral, the curvature must scale as $1/x_1$ for blow-up on the plane.

3. Reflectional symmetry

Reflectional symmetry of vorticity about the $x_i = 0$ Cartesian plane, $i = 1, 2, 3$, can be written as $\omega(I_i x) = -I_i \omega(x)$ where I_i is the identity matrix with the ith diagonal element negative. Flows with reflectional symmetry with respect to a plane have only normal vorticity in the plane. On the $x_1 = 0$ plane, for example, ω_1 is the only non-zero component of vorticity, and since u_1 is zero, the plane is also a stream surface. Only $u_{1,1}$, $u_{2,2}$, $u_{3,3}$, $u_{2,3}$ and $u_{3,2}$ are non-zero; hence, one of the eigenvectors of the strain rate matrix is also normal to the plane. On plane $x_1 = 0$, the vorticity equation reduces to

$$\frac{\partial \omega_1}{\partial t} + u_2\omega_{1,2} + u_3\omega_{1,3} = \omega_1 u_{1,1}. \tag{3.1}$$

With such an alignment of strain rate and vorticity it is natural to examine the behaviour of vorticity on such a symmetry plane for possible blow-up. In the remainder of this paper, the class of incompressible flows will be restricted to those with reflectional symmetry, and the possible blow-up location will be restricted to the symmetry plane. Flows will be further restricted to those which have at least one compact vortex tube which intersects the $x_1 = 0$ plane.

As can be seen in equation (2.3), it is clear that curvature must continually increase to have a strain rate which scales as local vorticity. This point is examined more closely by defining the local curvature on the symmetry plane. Curvature of a vector field line is the arclength derivative of the unit tangent, $\partial(\omega/|\omega|)/\partial s$. This reduces to $(0, \omega_{2,1}, \omega_{3,1})/\omega_1$ on the symmetry plane $x_1 = 0$. The local curvature on this plane is defined as $\kappa_2 = \omega_{2,1}/\omega_1$ and $\kappa_3 = \omega_{3,1}/\omega_1$.

The evolution of the local curvature of the vortex lines on the $x_1 = 0$ plane can be written

$$\frac{\mathrm{D}}{\mathrm{D}t}\begin{pmatrix}\kappa_2\\ \kappa_3\end{pmatrix} = \begin{bmatrix} (u_{2,2} - 2u_{1,1}) & u_{2,3} \\ u_{3,2} & (u_{3,3} - 2u_{1,1}) \end{bmatrix} \begin{pmatrix}\kappa_2\\ \kappa_3\end{pmatrix} + \begin{pmatrix}u_{2,11}\\ u_{3,11}\end{pmatrix}. \tag{3.2}$$

The first term on the right indicates that a positive out-of-plane strain rate, $u_{1,1}$, acts to decrease the curvature. This leads to a possible contradiction: curvature must increase for $u_{1,1}$ to increase, but large $u_{1,1}$ tends to decrease curvature.

One way to maintain nonlinear growth of curvature is for an in-plane deformation rate to be much larger than the out-of-plane strain rate. This will lead, however, to sheet formation and non-localization which contributes to depletion of nonlinearity.

The argument above applies to an isolated vortex tube that is symmetric with

respect to the $x_1 = 0$ plane. Now the class of flows will be further restricted to those with reflectional symmetry about the $x_2 = 0$ plane also. If the tube is brought close to the $x_2 = 0$ reflectional plane, the oppositely signed image tube sets up a dipolar arrangement which is subject to the Crow instability. As is well-known, the tubes collapse and, if viscosity is present, reconnect by diffusion of ω_2 across the $x_2 = 0$ plane (Kida & Takaoka 1994).

The assumption that the flow is invariant under the action of these symmetries leads to the definition of a 'fundamental domain' which is a subset of $\mathscr{R}^3$. For this class of flows, the strain rate integral, (2.3), can be written over the fundamental domain $x_2 \geqslant 0$, $x_1 \geqslant 0$. The strain rate at a point $(0, \bar{x}_2, \bar{x}_3)$ is then written in the fundamental domain as

$$u_{1,1}(0,\bar{x}_2,\bar{x}_3) = \frac{3}{4\pi} PV \int \left\{ \frac{x_1[(x_2-\bar{x}_2)\omega_3(x) + (x_3-\bar{x}_3)\omega_2(x)]}{[x_1^2+(x_2-\bar{x}_2)^2+(x_3-\bar{x}_3)^2]^{5/2}} + \frac{x_1[(x_2+\bar{x}_2)\omega_3(x) + (x_3-\bar{x}_3)\omega_2(x)]}{[x_1^2+(x_2+\bar{x}_2)^2+(x_3-\bar{x}_3)^2]^{5/2}} \right\} \mathrm{d}^3x. \quad (3.3)$$

These reflectional symmetries do not change the fact that the integrand contains only ω_2 and ω_3 and local axial strain rate must be produced by curvature of local vorticity. Hence, like in the case of the isolated tube, the behaviour of vortex line curvature is still the critical issue.

There is a controversy as to whether this configuration leads to finite-time blow-up. Filament computations of Siggia & Pumir (1985), Siggia (1985), Pumir & Siggia (1987), and Waele & Aarts (1994) have shown that there is an algebraic blow-up behaviour (with logarithmic corrections) during this collapse and up to the time when the closest distance to the $x_2 = 0$ plane is on the order of the filament core size (Biot-Savart desingularization length). It was then seen in the field computations of Pumir & Siggia (1990), and Shelley *et al.* (1993) that in that regime, core deformation and sheet formation occurred and the out-of-plane strain rate decorrelated with the local vorticity. Kerr (1993), however, using a specially filtered initial flow with high curvature, found this blow-up behaviour to continue in time for as long as he could compute.

The Taylor–Green vortex (Taylor & Green 1937) is a symmetric flow with reflectional symmetry about all three planes. Addition of the third symmetry plane still does not change the curvature restriction. Early work by Morf, Orszag & Frisch (1980) suggested that there exists a spontaneous singularity, but further study by Brachet *et al.* (1983, 1992) revealed only exponential behaviour.

The controversy over the dipolar-collapse problem may never be resolved due to the '$\epsilon < t_{crit} - T$' argument discussed in the introduction. In the next section, a somewhat unnatural symmetry is added to the problem which will allow a more natural strain rate/vorticity coupling to occur.

4. Octahedral symmetry

The class of incompressible flows is finally restricted to those flows that have reflectional symmetry about all three zero planes and a three-fold rotational symmetry about the diagonal. Again, this class of flows must have a vortex tube which intersects the $x_1 = 0$ plane. This symmetry can be visualized as follows: along a line from the origin through the point (1,1,1), the flow is invariant under a three-fold rotation by the angle $2\pi/3$. The rotational symmetry can be expressed as $\omega(Px) = P\omega(x)$, $PPP = I$

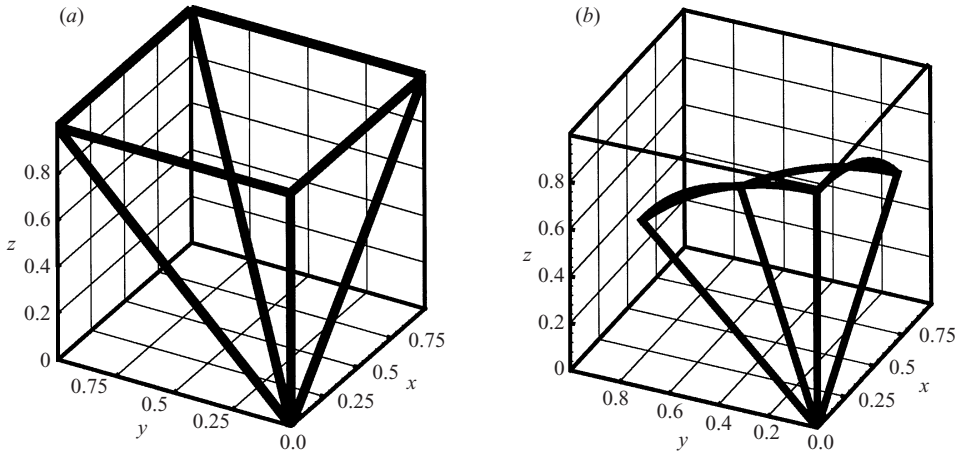

FIGURE 1. Two views of the fundamental domain, $\mathscr{F}$: (*a*) the right pyramid which is used in a Cartesian coordinate system; (*b*) a quadrilateral cone which is used in a spherical coordinate system.

where P is the permutation $P(x_1, x_2, x_3) = (x_3, x_1, x_2)$. Functions with the rotational symmetry are said to be invariant under the action of the octahedral symmetry group. Adding the reflections, it is known as the full octahedral symmetry group.

There are two reasons for such a severe restriction in the class of flows. The first, which will be shown in § 4.1, is that a new source of axial strain rate is produced by the images which is independent of the curvature of vortex lines. The second, which will be addressed in § 4.2, is that the origin is a degenerate critical point and the velocity field from the images causes a collapse towards the origin. This group is one of the simplest that restricts the origin to be a degenerate critical point.

The domain of integration of the strain rate integral in equation (2.2) can be reduced from $\mathscr{R}^3$ to a fundamental domain, $\mathscr{F}$, which is 1/24th the volume when the flow has symmetry. Let the full domain be a ball with radius $r \to \infty$. The three reflectional symmetries lead to a fundamental domain in the first octant only, which for spherical geometry is a triangular cone with vertex at the origin and a spherical triangle at radius r. Under the rotational symmetry, this fundamental domain can be reduced by a third. The spherical triangle can be divided into three equal parts by connecting great circles between the centroid and the three midpoints of the legs. The fundamental domain is then a cone with a spherical quadrilateral. One vertex of the quadrilateral is on the x_3-axis. A Cartesian, rather than spherical, fundamental domain can be constructed as a right pyramid $x_1 = [0, x_3], x_2 = [0, x_3], x_3 = [0, a]$ $a \to \infty$. See figure 1 for views of each of these fundamental domains.

4.1. *The out-of-plane strain rate*

In writing the strain rate integral within the fundamental domain only, there will be eight terms in the integrand from reflectional symmetries, and each of these terms will have three parts from rotational symmetry. The out-of-plane strain rate at the point $\bar{x} = (0, \bar{x}_2, \bar{x}_3)$ can be written

$$u_{1,1}(0, \bar{x}_2, \bar{x}_3) = \frac{3}{4\pi} \int_{\mathscr{F}} \{\omega_1(x)\mathscr{D}_1(\bar{x}, x) + \omega_2(x)[\mathscr{D}_2^*(\bar{x}, x) + \mathscr{D}_2(\bar{x}, x)] + \omega_3(x)[\mathscr{D}_3^*(\bar{x}, x) + \mathscr{D}_3(\bar{x}, x)]\} \, \mathrm{d}^3x \quad (4.1)$$

where the five kernels are

$$\mathscr{D}_1(0,\bar{x}_2,\bar{x}_3;x)=\frac{x_2(x_3-\bar{x}_2)}{[x_2^2+(x_3-\bar{x}_2)^2+(x_1-\bar{x}_3)^2]^{5/2}}+\frac{x_2(x_3-\bar{x}_2)}{[x_2^2+(x_3-\bar{x}_2)^2+(x_1+\bar{x}_3)^2]^{5/2}}$$
$$+\frac{x_2(x_3+\bar{x}_2)}{[x_2^2+(x_3+\bar{x}_2)^2+(x_1-\bar{x}_3)^2]^{5/2}}+\frac{x_2(x_3+\bar{x}_2)}{[x_2^2+(x_3+\bar{x}_2)^2+(x_1+\bar{x}_3)^2]^{5/2}}$$
$$-\frac{x_3(x_2-\bar{x}_3)}{[x_3^2+(x_1-\bar{x}_2)^2+(x_2-\bar{x}_3)^2]^{5/2}}-\frac{x_3(x_2-\bar{x}_3)}{[x_3^2+(x_1+\bar{x}_2)^2+(x_2-\bar{x}_3)^2]^{5/2}}$$
$$-\frac{x_3(x_2+\bar{x}_3)}{[x_3^2+(x_1-\bar{x}_2)^2+(x_2+\bar{x}_3)^2]^{5/2}}-\frac{x_3(x_2+\bar{x}_3)}{[x_3^2+(x_1+\bar{x}_2)^2+(x_2+\bar{x}_3)^2]^{5/2}},\tag{4.2}$$

$$\mathscr{D}_2^*(0,\bar{x}_2,\bar{x}_3;x)=-\frac{x_1(x_3-\bar{x}_3)}{[x_1^2+(x_2-\bar{x}_2)^2+(x_3-\bar{x}_3)^2]^{5/2}}-\frac{x_1(x_3-\bar{x}_3)}{[x_1^2+(x_2+\bar{x}_2)^2+(x_3-\bar{x}_3)^2]^{5/2}}$$
$$-\frac{x_1(x_3+\bar{x}_3)}{[x_1^2+(x_2-\bar{x}_2)^2+(x_3+\bar{x}_3)^2]^{5/2}}-\frac{x_1(x_3+\bar{x}_3)}{[x_1^2+(x_2+\bar{x}_2)^2+(x_3+\bar{x}_3)^2]^{5/2}},\tag{4.3}$$

$$\mathscr{D}_2(0,\bar{x}_2,\bar{x}_3;x)=\frac{x_3(x_1-\bar{x}_2)}{[x_3^2+(x_1-\bar{x}_2)^2+(x_2-\bar{x}_3)^2]^{5/2}}+\frac{x_3(x_1-\bar{x}_2)}{[x_3^2+(x_1-\bar{x}_2)^2+(x_2+\bar{x}_3)^2]^{5/2}}$$
$$+\frac{x_3(x_1+\bar{x}_2)}{[x_3^2+(x_1+\bar{x}_2)^2+(x_2-\bar{x}_3)^2]^{5/2}}+\frac{x_3(x_1+\bar{x}_2)}{[x_3^2+(x_1+\bar{x}_2)^2+(x_2+\bar{x}_3)^2]^{5/2}},\tag{4.4}$$

$$\mathscr{D}_3^*(0,\bar{x}_2,\bar{x}_3;x)=\frac{x_1(x_2-\bar{x}_2)}{[x_1^2+(x_2-\bar{x}_2)^2+(x_3-\bar{x}_3)^2]^{5/2}}+\frac{x_1(x_2-\bar{x}_2)}{[x_1^2+(x_2-\bar{x}_2)^2+(x_3+\bar{x}_3)^2]^{5/2}}$$
$$+\frac{x_1(x_2+\bar{x}_2)}{[x_1^2+(x_2+\bar{x}_2)^2+(x_3-\bar{x}_3)^2]^{5/2}}+\frac{x_1(x_2+\bar{x}_2)}{[x_1^2+(x_2+\bar{x}_2)^2+(x_3+\bar{x}_3)^2]^{5/2}},\tag{4.5}$$

$$\mathscr{D}_3(0,\bar{x}_2,\bar{x}_3;x)=-\frac{x_2(x_1-\bar{x}_3)}{[x_2^2+(x_3-\bar{x}_2)^2+(x_1-\bar{x}_3)^2]^{5/2}}-\frac{x_2(x_1-\bar{x}_3)}{[x_2^2+(x_3+\bar{x}_2)^2+(x_1-\bar{x}_3)^2]^{5/2}}$$
$$-\frac{x_2(x_1+\bar{x}_3)}{[x_2^2+(x_3-\bar{x}_2)^2+(x_1+\bar{x}_3)^2]^{5/2}}-\frac{x_2(x_1+\bar{x}_3)}{[x_2^2+(x_3+\bar{x}_2)^2+(x_1+\bar{x}_3)^2]^{5/2}}.\tag{4.6}$$

The important points of the above (regrettably long) expressions are that $\omega_1(x)$ is now present in the integrand of equation (4.2) and that the associated kernel, $\mathscr{D}_1$, which comes solely from the rotated images, is smooth in the fundamental domain as long as ($\bar{x}_2 < \bar{x}_3$). The smooth kernels $\mathscr{D}_2$ and $\mathscr{D}_3$ are also from rotated images,

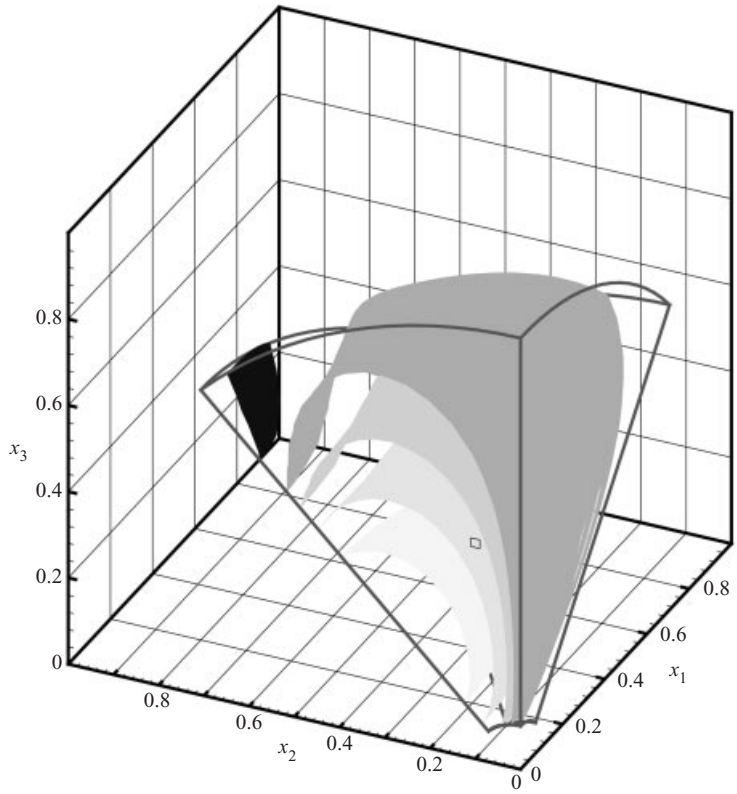

FIGURE 2. Isosurfaces of the $\mathscr{D}_1(\bar{x}, x)$ kernel in the fundamental cone. Contour levels are 0, 1, 2, 4, and 8 from dark to light with [−0.5, 20] being the range. The region of negative $\mathscr{D}_1$ is to the left of the black surface. The square marks the spot where $(0, \bar{x}_2, \bar{x}_3)$ and $\bar{x}_2 = 0.1$ and $\bar{x}_3 = 0.5$. Note that $\mathscr{D}_1$ is a weak function of x_1 implying that a mildly curved vortex tube centred at $(0, \bar{x}_2, \bar{x}_3)$ will be immersed in a nearly constant positive kernel field. Similar positive fields are found as $\bar{x}_3/\bar{x}_2$ is varied.

whereas $\mathscr{D}_2^*$ and $\mathscr{D}_3^*$ contain the original singular kernels and the contributions from reflected images.

The kernel $\mathscr{D}_1$ is positive under certain conditions. At $x = (0, \bar{x}_2, \bar{x}_3)$ it is

$$\mathscr{D}_1 = 2(\bar{x}_3^2 - \bar{x}_2^2)\left[\frac{1}{[\bar{x}_2^2 + (\bar{x}_3 - \bar{x}_2)^2 + \bar{x}_3^2]^{5/2}} - \frac{1}{[\bar{x}_2^2 + (\bar{x}_3 + \bar{x}_2)^2 + \bar{x}_3^2]^{5/2}}\right] \tag{4.7}$$

which is positive if $\bar{x}_3 > \bar{x}_2$. The isosurfaces of the kernel $\mathscr{D}_1$ are plotted in figure 2 in the fundamental conical domain. The square marks the spot $(0, \bar{x}_2, \bar{x}_3)$. In this example $\bar{x}_2 = 0.1$ and $\bar{x}_3 = 0.5$. Similarly shaped positive surfaces occur for any $\bar{x}_2$ and $\bar{x}_3$ provided $\bar{x}_2 < \bar{x}_3$. Contour levels are 0, 1, 2, 4 and 8 from dark to light. The only negative volume is to the left of the black surface.

Recall that the class of flows under consideration has a compact vortex tube. Let this vortex tube intersect the $x_1 = 0$ plane normally with its centroid at $(0, \bar{x}_2, \bar{x}_3)$. Define a length scale, L, as the distance from the centroid of the vortex tube to the origin ($L = \sqrt{\bar{x}_2^2 + \bar{x}_3^2}$). The vortex tube is assumed to have mild curvature, $\rho \geqslant L$. Following the vortex lines, the tube then extends across the fundamental domain and exits on the opposite side boundary, much like the positive level sets of $\mathscr{D}_1$ in figure 2. The tube enters the other rotational boundary oriented mostly in the x_3-direction.

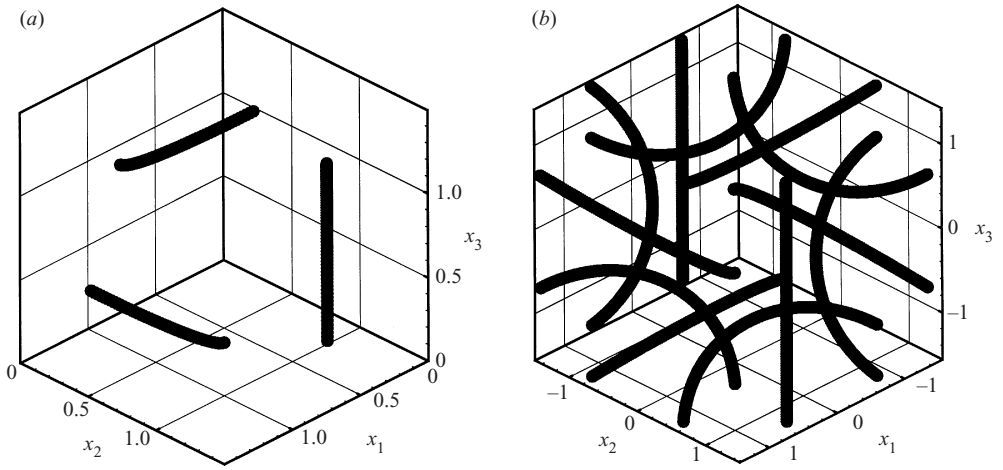

FIGURE 3. Plots of the space curve ($x_1 = s - \epsilon^2 s^3/6 + \cdots$, $x_2 = \cos v + \epsilon s^2 \cos(\mu)/2 + \cdots$, $x_3 = \sin v + \epsilon s^2 \sin(\mu)/2 + \cdots$) plus images from octahedral symmetry. Parameters are $\epsilon = 1/2$, $v = 0.43\pi$ and $\mu = \pi/4$. (*a*) The first octant only, and (*b*) the whole cube with side length 3.

Because the rotational images are at a distance proportional to L from $(0, \bar{x}_2, \bar{x}_3)$, their influence on the strain rate at this point can be estimated through the vortex filament approximation. The integral

$$\int [\mathscr{D}_1(x, \bar{x})\omega_1(x) + \mathscr{D}_2(x, \bar{x})\omega_2(x) + \mathscr{D}_3(x, \bar{x})\omega_3(x)]\, \mathrm{d}^3x \tag{4.8}$$

over the fundamental domain is approximated by a one-dimensional integral over the arclength of a space curve $x(s)$ expanded about the symmetry plane. Letting the radius of curvature and the torsion on the symmetry plane be ρ and τ, and the arclength derivative be denoted by an overdot, the position of the vortex filament has the form

$$\left.\begin{aligned} x_1 &= \rho\left[\left(\frac{s}{\rho}\right) - \frac{1}{6}\left(\frac{s}{\rho}\right)^3 + O\left(\frac{s}{\rho}\right)^5\right], \\ x_2 &= \bar{x}_2 + \rho_2\left[\frac{1}{2}\left(\frac{s}{\rho}\right)^2 - \frac{\rho\ddot{\rho}+1}{24}\left(\frac{s}{\rho}\right)^4\right] - \rho_3\left[\frac{\rho^2\dot{\tau}}{24}\left(\frac{s}{\rho}\right)^4\right] + O\left(\rho\frac{s}{\rho}\right)^6, \\ x_3 &= \bar{x}_3 + \rho_3\left[\frac{1}{2}\left(\frac{s}{\rho}\right)^2 - \frac{\rho\ddot{\rho}+1}{24}\left(\frac{s}{\rho}\right)^4\right] + \rho_2\left[\frac{\rho^2\dot{\tau}}{24}\left(\frac{s}{\rho}\right)^4\right] + O\left(\rho\frac{s}{\rho}\right)^6, \end{aligned}\right\} \tag{4.9}$$

where ρ_2 and ρ_3 are the radii of curvature, $\rho^2 = \rho_2^2 + \rho_3^2$. Lengths are then normalized with respect to L, the scaled curvature $\epsilon = L/\rho$ is defined, and two angles μ and v are defined as $(\bar{x}_2, \bar{x}_3) = (\cos v, \sin v)$ and $(\rho_2, \rho_3) = \rho(\cos\mu, \sin\mu)$. Figure 3 shows the position of the filament and images in the first octant and the whole plane.

The axial strain rate $u_{1,1}$ at the point $(0, \bar{x}_2, \bar{x}_3)$ from the rotated images only can be expanded in powers of ϵ (scaled curvature) as

$$u_{1,1}^{image} = \frac{\Gamma}{L^2}[c_0(v) + c_1(\mu, v)\epsilon + O(\epsilon^2)]. \tag{4.10}$$

The functions c_0 and c_1 are shown in figure 4 for $\pi/4 \leqslant v \leqslant \pi/2$; the solid line is c_0 and the broken lines are c_1 evaluated at $\mu = \{0, \pi/4, \pi/2\}$. Integration is to infinity, but since the integrands are highly localized (scaling as $|x/L|^{-5}$), integration across the

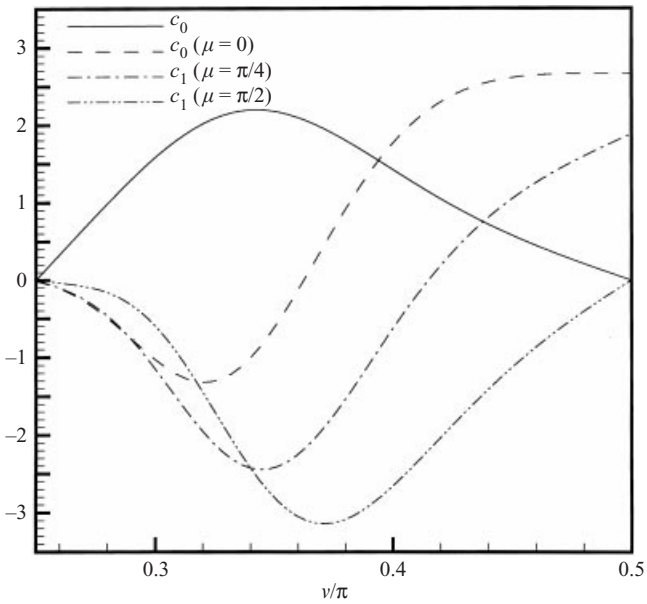

FIGURE 4. The zeroth-, $c_0(v)$, and first-order, $c_1(\mu, v)$, terms in the expansion of out-of-plane strain rate on the symmetry plane due to images only. The integral is estimated using the filament approximation and a space curve expansion. The expansion parameter is $\epsilon = L/\rho$. The angles v and μ describe the intersection of the filament with the symmetry plane and direction of curvature, respectively.

fundamental domain produces the major contribution to the integral. The function c_0 is the strain rate produced by the rotational images of a straight filament. It is positive for $\bar{x}_3 > \bar{x}_2$. The effect of mild curvature can be seen in the function $c_1(\mu, v)$. Positive curvature causes the filament to move away from $(0, \bar{x}_2, \bar{x}_3)$ more quickly than if it is straight. The contribution to the strain rate is, therefore, generally negative. Even in the worst case which occurs when $\rho_3 = \rho\,(\mu = \pi/2)$, the strain rate is positive for $\pi/4 < v < \pi/2$ if the scaled curvature, ϵ, is less than one half. It is interesting to note that for $\mu < \pi/2$, curvature has a positive contribution to the strain rate for some range of v, e.g. for $\mu = \pi/4$, $c_1 > 0$ for $v > 4\pi/10$. This is due to the fact that strain rate is larger in front of a wider dipole. In the next section where numerical evidence is given, curvature is indeed mild and v and μ are in the range where curvature enhances positive strain rate.

There are two results from this filament analysis. First is that the strain rate from the images is positive in the limit of zero curvature provided $\bar{x}_3 > \bar{x}_2$. Recall that when curvature is zero, the strain rate produced by the fundamental vortex and reflections is zero.

The other result is that the strain rate from the rotational images scales as L^{-2}. If the vortex tube were to move towards the origin by a factor α, $L \to \alpha L$, and the tube remains coherent with mild (scaled) curvature, the axial strain rate experienced by the tube on the symmetry plane from the images would increase by the inverse square, $u_{1,1} \to u_{1,1}/\alpha^2$.

Of course, the evidence above is from a static filament model. It will give the leading behaviour only if core size is small with respect to interfilament distance and radius of curvature and if the dynamic behaviour is self-similar.

While the filament/space curve expansion is not entirely appropriate for the esti-

mation of the strain rate due to the singular terms because of core deformation, it is nevertheless interesting to examine the local strain rate integral under this approximation. Letting $\rho\theta = s$, the integral of $u_{1,1}$ on the plane due to the fundamental vortex only becomes

$$u_{1,1}^{singular} = \Gamma\,\dot{t}\int_0^{\theta_{max}} [\tfrac{1}{24}\theta + O(\theta^3)]\,\mathrm{d}\theta. \tag{4.11}$$

The fact that a plane filament does not strain itself is borne out by the torsion multiplicative factor. (Note that torsion is an odd function with respect to the symmetry plane, and arclength derivative of torsion is the relevant parameter.) The integrand is not singular but a smooth non-local function of θ. The arclength derivative of the torsion must become singular in order for the axial strain rate to become singular from local effects.

The in-plane strain rates $u_{2,2}$ and $u_{3,3}$ can be examined in a manner similar to that of $u_{1,1}$. For the same class of flows and $\bar{x}_3 > \bar{x}_2$ the kernels analogous to $\mathscr{D}_1$ are smooth and negative throughout the fundamental domain. This suggests that the normal direction is the eigenvector of the largest (and perhaps the only) positive eigenvalue of the rate of strain matrix.

In summary, for a flow invariant under the action of the full octahedral symmetry group and a vortex tube intersecting a symmetry plane at a distance L from the origin, the axial strain on the vortex at the symmetry plane has a component from the rotational images which is positive for a mildly curved tube and scales like ΓL^{-2}.

4.2. *The velocity field and the geometry of the critical point*

In the previous subsection it was shown that rotated images of the coherent vortex tube provide a source of axial strain. Reliance on the images for blow-up then requires them to continually move closer to the fundamental, or for the whole configuration to move towards the origin in such a way that the vortex orientation is preserved ($L \to 0$). This can be accomplished through a self-similar collapse to the origin. Note that the collapse can be asymptotic in nature as long as a suitable matching region can connect an outer flow with the inner collapse. In this section the velocity field and the geometry of the critical point will be examined for flows with full octahedral symmetry.

The most general incompressible flow with this symmetry is severely restricted around the origin. The assumption of reflectional symmetry on the three zero planes restricts the axes to be streamlines. Applying incompressibility, the origin becomes a hyperbolic critical point, and the axes are the stable and unstable directions. Enforcing the three-fold rotational symmetry about the diagonal, further restricts all axes to be similar. The origin thus becomes a degenerate critical point.

In a Taylor expansion of the velocity about the origin, the first-order terms are zero from the degeneracy. The expansion is odd in r so the first non-zero terms will be of third order. Of the ten possible coefficients involved in the expansion at third order, only two are independent and can be separated with a toroidal and poloidal decomposition.

The poloidal (radial) velocity has the form $[x^4 + y^4 + z^4 - 3(x^2y^2 + y^2z^2 + z^2x^2)]/r + O(r^5)$. This function has oppositely signed extrema on the axes and diagonals, which means that the six axes are the incoming streamlines and the eight diagonals are the outgoing streamlines (or vice versa depending on the sign of the multiplying coefficient). The acute angle between incoming and outgoing streamlines is $\arccos(1/\sqrt{3})$.

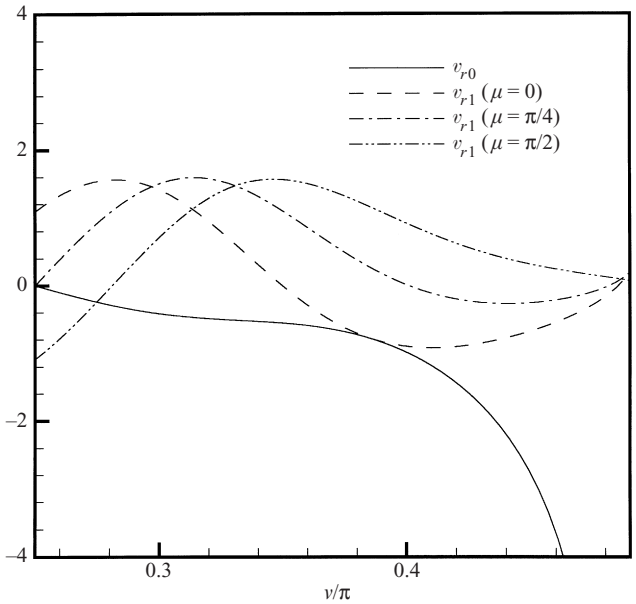

FIGURE 5. The zeroth-, $v_{r0}(v)$, and first-order, $v_{r1}(\mu, v)$, terms in the expansion of radial velocity on the symmetry plane. The velocity is estimated using the filament approximation for non-local vorticity and local induction approximation for local effects. The expansion parameter is $\epsilon = L/\rho$. The angles v and μ describe the intersection of the filament with the symmetry plane and direction of curvature, respectively. The core size is $L/5$.

That this angle is acute means that if collapse to the origin does occur then the local radius of curvature of the vortex lines will go to zero.

The toroidal term can be expressed using the radial vorticity, which has the form $xyz/r+O(r^4)$. This means that the streamlines on the sphere are closed and concentric, with the centre at the diagonal point. The flow is confined to the octant and swirls around the diagonal. The swirl in adjacent octants is oppositely signed.

While this expansion is valid only close to the origin, the idea of a collapse in an incompressible flow can be visualized. The down-welling flow is near the axes and a swirling up-welling flow is near the diagonals.

The velocity field at a distance L from the origin is certainly not well represented by the first term of the Taylor series given above. To examine the velocity there, the filament model of the previous subsection is used. As before the rotational images will be represented as filaments. The reflectional images will also be represented by filaments, and the local induction approximation will be used for the velocity of the fundamental.

The radial and azimuthal velocities, u_r and u_θ at the point $(0, \bar{x}_2, \bar{x}_3)$ can again be expanded in powers of ϵ from the Biot-Savart law with octahedral symmetry as

$$u_r = \frac{\Gamma}{L}[v_{r0}(v) + v_{r1}(\mu, v)\epsilon + O(\epsilon^2)], \quad u_\theta = \frac{\Gamma}{L}[v_{\theta 0}(v) + v_{\theta 1}(\mu, v)\epsilon + O(\epsilon^2)]. \tag{4.12}$$

The functions are shown in figures 5 and 6 for $\pi/4 \leqslant v \leqslant \pi/2$; the solid line is the zeroth-order term and the broken lines are the first-order terms evaluated at $\mu = 0, \pi/4, \pi/2$. Integration is to infinity, and the integrands are again highly localized. The core size is kept fixed at $L/5$, but results depend only weakly on this parameter.

Looking first at the radial velocity, a straight filament produces only a velocity

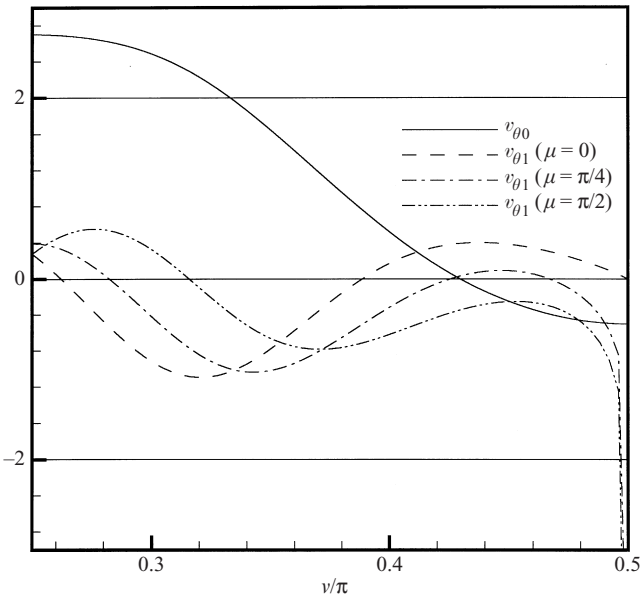

FIGURE 6. The zeroth-, $v_{\theta 0}(v)$, and first-order, $v_{\theta 1}(\mu, v)$, terms in the expansion of azimuthal velocity on the symmetry plane.

towards the origin. The general effect of curvature is to add positive velocity, but there is a range of μ where there is a negative contribution.

The leading behaviour of azimuthal velocity is positive for lower values of v and negative for higher values. Note that for a dipole or quadrupole alone, the azimuthal velocity is always negative. The positive contribution is due to the rotational images, particularly the jet between the image dipoles. The first-order curvature effect adds little to this behaviour.

This model thus predicts a certain angular location of the filament, $v \approx 0.43\pi$, where the velocity is only towards the origin. The filament will accelerate since the velocity there has the form $\dot{L} \sim 1/L$ with the solution $L \sim \sqrt{t_c - t}$. The critical angle is attracting since the derivative of azimuthal velocity with respect to v is negative there.

This model predicts that a mildly curved filament placed near this point in this symmetry space is trapped to move towards the origin. The fact that v is close to $\pi/2$ means that the fundamental vortex tube and image across the $x_2 = 0$ plane form a dipole and excite the radial velocity mode with down-welling at the axes. The three tubes in the first octant moving away radially from the origin excite the toroidal mode.

5. Evidence from numerical simulation

In the last section, the coupling of the strain rate and the vorticity on the symmetry plane was shown for flows with octahedral symmetry. Such a flow was constructed simply by having a vortex tube with mild curvature intersect the $x_1 = 0$ plane. In this section, previous simulations with such a symmetry will be analysed. In particular, the strain rate kernels will be examined to see the extent of the coupling.

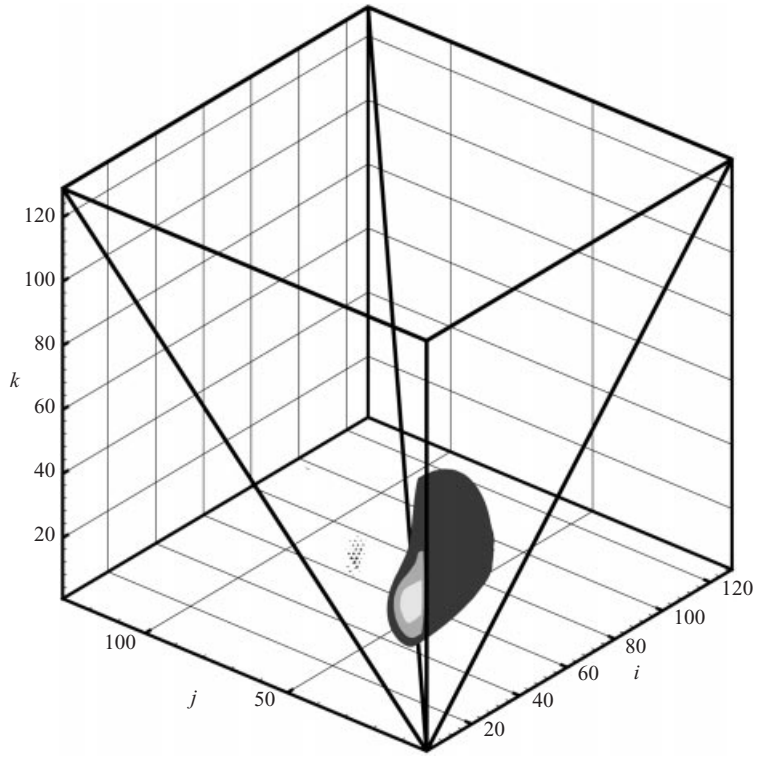

FIGURE 7. Isosurfaces of vorticity magnitude for $t = 1.5$ in the fundamental pyramid. Contours are 21, 17, 11 for light to dark with 23 being the overall maximum. There is a slight dusting as the isosurface comes through the rotational boundary.

5.1. *Pseudo-spectral simulations*

In the numerical studies of Boratav & Pelz (1994), an initial flow of the form

$$\omega_1 = 3\cos x_1 (\sin 3x_2 \sin x_3 + \sin x_2 \sin 3x_3) - 2\cos 3x_1 \sin x_2 \sin x_3 \qquad (5.1)$$

evolves into a collapsing 'dodecapole' arrangement as conjectured in the previous section. This highly symmetric flow was developed by Kida (1985) in order to increase the ratio of range of scales in a turbulent flow to the computational resources. It collapses towards the origin in a visually self-similar way up to the time when the simulation can no longer be trusted. The critical time is estimated to be about 2, and the time when the width of the analyticity strip equals the grid size is $t = 1.4$ (for an effective resolution of 1200^3 Fourier modes in an Euler simulation). Data collected at times much beyond this time should be considered only in the qualitative sense. The energy spectrum for times up to $t = 1.4$ tends to k^{-3}. The vorticity $|\omega|_\infty$ has a $1/(t_{crit} - t)$ behaviour for 2–3 orders of magnitude albeit for times extending into the critical range. The strain rate/vorticity coupling of this flow for $t = 1.5$ is examined below.

In figure 7 isosurfaces of vorticity magnitude are shown in the fundamental domain only. The maximum vorticity is 23 and the contours are 21, 17, and 11 from light to dark. The vortex tube is coherent as it intersects the $x_1 = 0$ plane. The typical head/tail arrangement can be seen in the contours of the cross-section. It extends

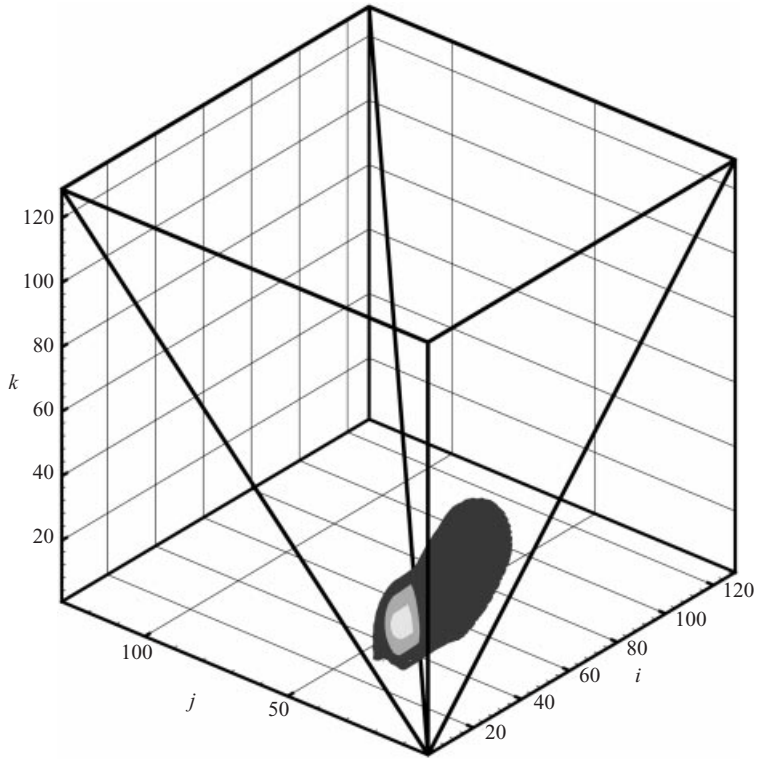

FIGURE 8. Isosurfaces of the strain rate integrand: $\mathscr{D}_1(x=0,\bar{x}_2,\bar{x}_3;x)\omega_1(x)$ in the fundamental domain. Contours are 64, 32, 16 for light to dark with 89 being the overall maximum.

from the $x_1 = 0$ plane normally with decreasing magnitude but mild curvature. With reference to the preceding section, the angle v is close to $\pi/2$ and μ is close to zero. Lower isosurfaces show the tube exiting the far rotational boundary and re-entering the other rotational boundary. There is another vortex structure near the point $(\pi/2, \pi/2, \pi/2)$, but this is not shown. The point with maximum positive vorticity is $(0, 7, 21)(\pi/128)$, and this will be defined to be the point $(0, \bar{x}_2, \bar{x}_3)$.

To understand the extent of the coupling, the field $\mathscr{D}_1(0, \bar{x}_2, \bar{x}_3; x)\omega_1(x)$, as defined in equation (4.3), for the fundamental domain is shown in figure 8. The maximum value in the field is 89, and the isosurfaces are 64, 32, and 16 from light to dark. The integrand is positive and the contours envelop the vortex tube shown in figure 7. The large degree of positive correlation between the $\mathscr{D}_1$ and $\omega_1(x)$ fields suggests that a large axial strain rate is produced by the rotational images.

To illustrate the strain rate budget as defined in equation (4.2), four contour plots are shown in figure 9. The time is again 1.5. The area shown is a small part of the plane $x_1 = 0$ for which $0 \leqslant x_2 \leqslant 5/32$ and $3/16 \leqslant x_3 \leqslant 5/16$ expressed in fractions of domain length.

Figure 9(*a*) shows the contours of ω_1; (*b*) shows a contour plot of out-of-plane strain rate $u_{1,1}$ that is acting on the vorticity. Contours are ragged indicating that as gradients get steeper, lack of resolution will soon prevent further integration. In the region of 'high' vorticity, defined by $\omega_1 > 20$, the strain rate is nearly vertically stratified. It increases in the vertical direction from about 1.8 to 2.7.

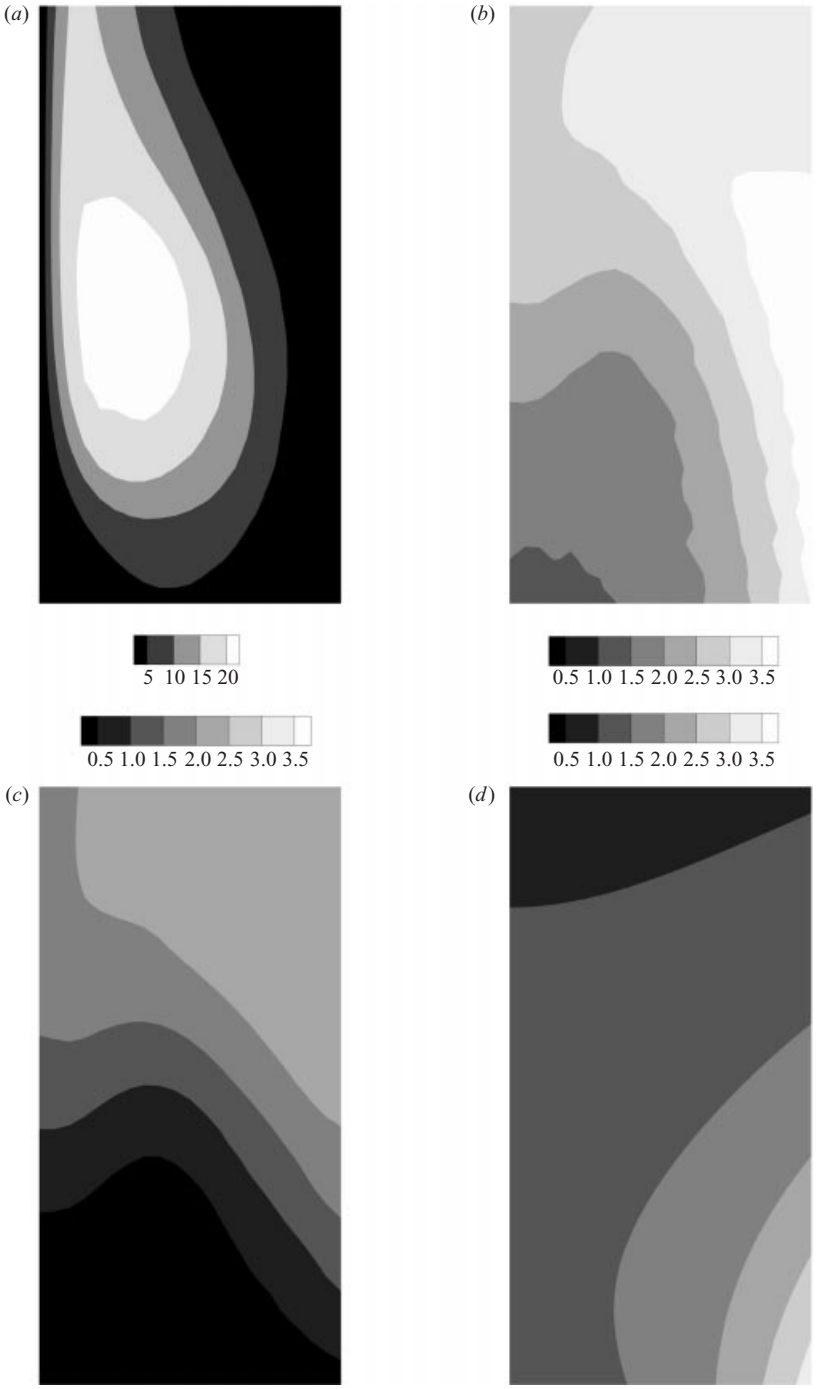

FIGURE 9. Contour plots from a pseudo-spectral simulation for time 1.5, $x_1 = 0$, $0 \leqslant x_2 \leqslant 5/32$, $3/16 \leqslant x_3 \leqslant 5/16$: (*a*) vorticity ω_1, (*b*) axial strain rate $u_{1,1}$, (*c*) axial strain rate due to the fundamental and reflectional vorticity, and (*d*) axial strain rate due to rotational image vorticity.

Figure 9(*c*) shows contours of the out-of-plane strain rate due to the fundamental vorticity and reflectional images. This is found by integrating $\mathscr{D}_2^*\omega_2 + \mathscr{D}_3^*\omega_3$ as defined in equations (4.4) and (4.6). Contours are smoother due to integration. Figure 9(*d*) shows contours of out-of-plane strain rate due to the rotational image vorticity, or the integration of $\mathscr{D}_1\omega_1 + \mathscr{D}_2\omega_2 + \mathscr{D}_3\omega_3$ as defined in equations (4.3), (4.5) and (4.7).

In the region of high vorticity, the local and reflection strain rate contours are also horizontally stratified with a range of about 0.03 to 1.7 increasing upwards. The contours of strain rate from the rotational images are very different. In the high-vorticity region, the distribution is more constant ranging from 1 to 1.5 and the strain rate increases to the lower right. At this time, the rotational images produce a slightly higher integrated strain rate over the high-vorticity region than the fundamental and reflectional images.

A coupling coefficient can be defined as the ratio of strain rate to vorticity in the region of high vorticity on the plane. If the coefficient is constant in time, then there is a linear coupling between vorticity and strain rate. If it persists, then blow-up will occur in a finite time. At the time of 1.5, the coupling coefficient is about 1/10. At a time of 1.6 (not shown), it is still about a tenth, but the ratio of rotational to fundamental and reflectional contributions is larger than at $t = 1.5$.

Because the raggedness of the derivative fields is symptomatic of the progressive loss of resolution with time, quantitative analysis of scaling is useless. The main result is that at the times analysed, in the region where the coherent vortex tube intersects the reflectional plane, a significant part of the axial strain rate budget comes from the rotational vorticity.

A view of the velocity field on the symmetry plane is seen in figure 10. The vorticity contours are overlaid with velocity vectors and a few streamlines. There are a number of interesting points here. All streamlines end at the stable focus. A strong horizontal velocity is created by the rotational image vorticity, and it causes a nearly radial separatrix to form. The focus is not at the centre of the vortex, but is shifted due to the flow produced by the images. Nearly all of the vortex is immersed in a flow towards the origin. This figure supports what was found in the filament model in the last section: that the vortex is trapped and collapses towards the origin.

5.2. *Vortex filament calculations*

A simulation of the six dipole configuration was done with a standard vortex filament method by Pelz (1997). Results were similar to the pseudo-spectral computations; however, because the filament method is effectively one-dimensional, integration to times much closer to the critical time can be accomplished, and the locally self-similar solution can be analysed quantitatively. The strain rate/vorticity coupling for this simulation is examined below.

The data from the simulation are the position of the endpoints of the piecewise linear vortex segments at each time step, $x_1(s_i, t^n), x_2(s_i, t^n), x_3(s_i, t^n)$, where s is the arc-length and $i = 0, 1, \ldots, I$ is the segment index. The data are given at discrete times t^n, $n = 0, 1, \ldots$. Also given is the local core radius or desingularization length, $\sigma(s_i, t^n)$. The lengths of the segments are kept approximately equally spaced and much smaller than L and ρ by frequent spline interpolation. The time step is scaled on the inverse of maximal strain rate. The core size evolves based on the local strain rate. The plane $x_1 = 0$ is chosen to be the beginning of the arclength: $\bar{x}_2(t^n) = x_2(s_0 = 0, t^n)$ and $\bar{x}_3(t^n) = x_3(s_0 = 0, t^n)$. Figure 11 shows the position of the filament at a late time in the evolution. The surface plotted is the cylinder around the filament with radius

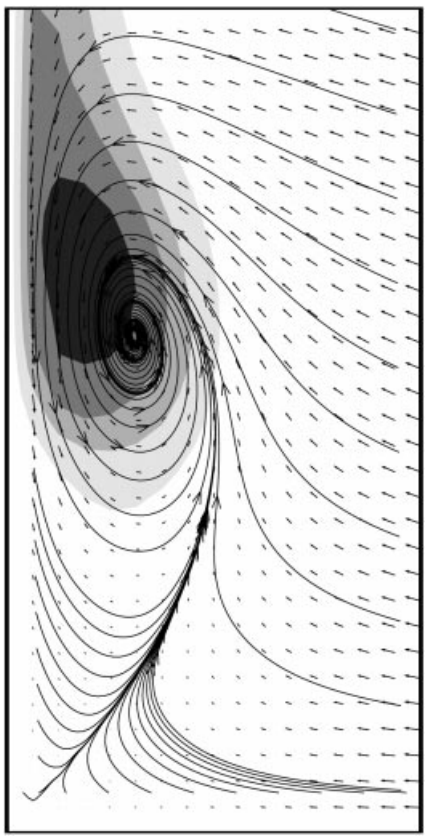

FIGURE 10. Vorticity contours (5,10,15,20 from light to dark) on the symmetry plane with velocity vectors and streamlines.

equal to half of the core size. Note the similarity with the filaments in figure 3. It is found that ϵ is about 0.44, ν is about 0.43π and $\mu < \pi/4$.

In evaluating the integral of the strain rate, $u_{1,1}(0, \bar{x}_2, \bar{x}_3)$, the volume integral is reduced to an arclength integral by the approximation that $\omega = \zeta\Gamma/(\pi\sigma^2)$, where ζ is the unit tangent to vortex lines and Γ is the circulation. Dividing the integrand by the vorticity of the tube at the symmetry plane, $\omega(0) = \Gamma/(\pi\sigma^2(0))$, the coupling coefficient between strain rate and vorticity at the point $(0, \bar{x}_2, \bar{x}_3)$ is defined to be the integral of

$$f(s) \equiv \sigma^2(0)\mathscr{D}_1(x(0), x(s_i))\zeta_1(s_i) \tag{5.2}$$

over the arclength of the filament. If the arclength integral of f is constant in time, then vorticity and axial strain rate are linearly related.

In figure 12 a plot of the function f versus arclength$/L$ is shown for a number of different times during the simulation. The plot shows that the integrand is positive and apparently converges to a particular function with time. Initially L is almost 4.6 so L decreases by four orders. (The computation required a day on a workstation and could of course be continued.)

The integral of f in this plot is the coupling between vorticity and axial strain rate. Trapezoidal integration yields the sequence {0.0407, 0.0675, 0.0697, 0.0686, 0.0684,

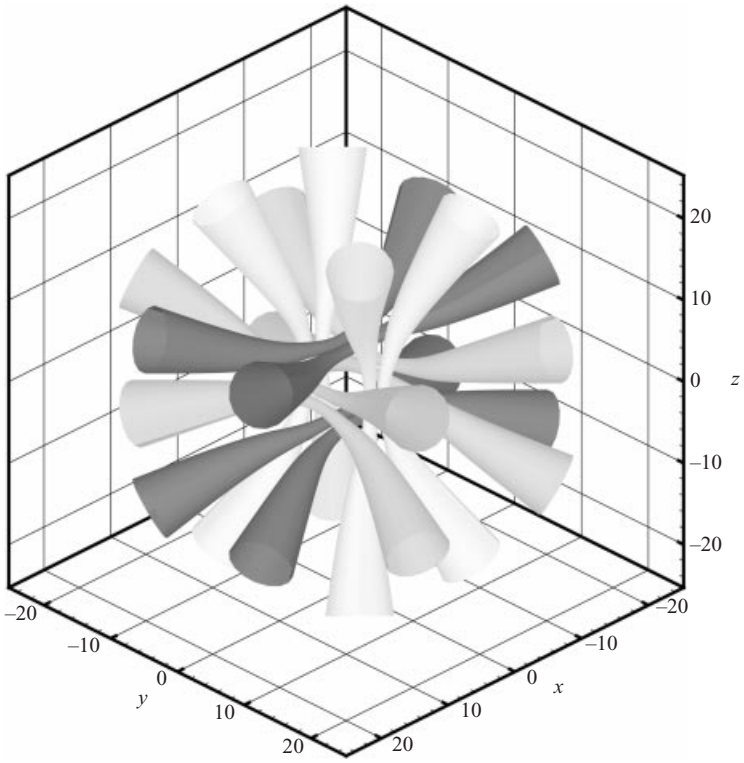

FIGURE 11. Location of the vortex filament at a late time for the complete domain shown to a radius of about $5L$. The width of the tube represents one half the core radius.

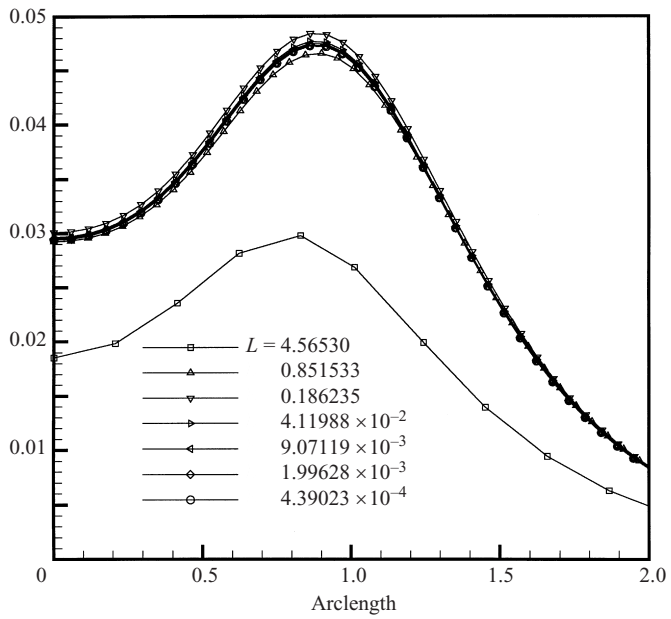

FIGURE 12. The integrand of the strain rate divided by the vorticity on the plane, as a function of arclength of the filament. Different times are indicated by the decreasing L values. All quantities are normalized by L. The integral of this curve gives the coupling coefficient.

0.0681, 0.0680} for the times shown. Thus for the filaments, there is linear coupling between vorticity and axial strain rate at $(0, \bar{x}_2, \bar{x}_3)$ as $t \to t_{crit}$.

6. Discussion

This paper concerns the problem of whether finite-time blow-up solutions exist for the equations governing the motion of an incompressible, inviscid fluid. The flow is assumed to be invariant under the octahedral symmetry group. In addition, a compact vortex tube was constructed to intersect (normally) with a reflectional symmetry plane ($x_1 = 0$). The tube has mild curvature so the vorticity is mainly in the x_1-direction as it extends across the fundamental domain. By writing the strain rate integral in the fundamental domain only, and examining the axial strain rate on the symmetry plane, the strain rate induced by the rotational images was shown to be proportional to ω_1, while the contributions from the fundamental and reflectional images were not; hence, the rotational images provide a fundamentally new source of strain rate.

Estimating the contribution of the image vortices to the axial strain rate on the fundamental using a filament model and an expansion in curvature, the strain rate was found to be proportional to Γ/L^2, where L is the distance to the origin of the vortex tube in the symmetry plane. A collapse to the origin as $L \sim \sqrt{t_c - t}$ would be accompanied by the strain rate scaling as $(t_c - t)^{-1}$. It is crucial, therefore, that the velocity field support such a collapse dynamic. Estimating the velocity using a filament model for images and the local induction approximation (LIA) for the fundamental, showed that there is a location for the fundamental where the velocity is only towards the origin. Furthermore, this radial velocity scales as L^{-1} so that $L \sim \sqrt{t_c - t}$.

The assumptions that lead to this scaling are that curvature stays mild compared with the distance to the origin, that the tube stays coherent and that the collapse is self-similar locally. That the curvature stays mild is reasonable since it is shown that large positive axial strain rate tends to decrease curvature. Coherence is also reasonable given that strain rate is produced by an integral effect at a distance. Axial strain rates that are positive, and in-plane strain rates induced by the rotational images that are negative also support coherence.

It is also reasonable that the flow approaches a local self-similarity. First, the symmetries cause a shielding of the inner region from the outer, exemplified by the rapid fall-off of the Biot-Savart and strain rate kernels. Also, the part of the vortex tube on and near the symmetry plane accelerates towards the origin leaving the complementary part of the tube to align radially and asymptote to the outgoing manifold – the diagonal. Radial vortex lines induce a flow on the sphere which further isolates the inner region from the outer. This scenario suggests that the outer edge of the self-similar region also collapses, which then does not violate the theorem of Necas, Ruzicka & Sverak (1996) and possibly that of Tsai (1998) on the non-existence of self-similar solutions for the Navier–Stokes equations.

The reliance on estimates from filament models sets the scaling to be the one suggested by Leray (1934) for an inner solution:

$$u(x,t) = \frac{\sqrt{\lambda}}{\sqrt{t_{crit} - t}} U(\xi), \quad x = \sqrt{\lambda(t_{crit} - t)}\xi, \tag{6.1}$$

where U is smooth and λ is a constant with units of circulation.

In conclusion, general flows as well as those with reflectional symmetries have the property that the axial strain rate is a function of the field of orthogonal components of vorticity. Strain/vorticity coupling then requires severe constraints on vortex line

curvature. By adding a rotational or permutation symmetry, axial strain rate becomes a (non-singular) function of the full vorticity not just the orthogonal components. If the flow approaches a self-similar collapse, the axial strain rate becomes proportional to the vorticity and the blow-up situation $\mathrm{D}\omega/\mathrm{D}t \sim \omega^2$ occurs. While there is evidence of such a collapse from models and simulations, future analysis should concentrate on whether such a flow with octahedral symmetry collapses locally about the degenerate critical point.

The work also suggests that other blow-up flows may be constructed using symmetries. The vortex dipole, because of the strain rate field it produces and its induced motion, is an important component (see the model of Moffatt 2000). Reflectional symmetries produce dipoles naturally. The proper phase relation can be produced by adding rotational symmetries. While rotation by any angle is supported, the three-fold one may be the simplest.

Thanks to John Greene, Charles Fefferman, Olus Boratav and Yuriy Gulak for helpful comments on the manuscript.

REFERENCES

Beale, J. Y., Kato, T. & Majda, A. 1984 Remarks on the breakdown of smooth solutions for the 3-D Euler equations. *Commun. Math. Phys.* **94**, 61.

Boratav, O. N. & Pelz, R. B. 1994 Direct numerical simulation of transition to turbulence from a high-symmetry initial condition. *Phys. Fluids* **6**, 2757–2784.

Boratav, O. N., Pelz, R. B. & Zabusky, N. J. 1992 Reconnection in orthogonally interacting vortex tubes: Direct numerical simulations and quantifications. *Phys. Fluids* A **4**.

Brachet, M. E., Meiron, D. I., Orszag, S. A., Nickel, B. G., Morf, R. H. & Frisch, U. 1983 Small-scale Structure of the Taylor-Green Vortex. *J. Fluid. Mech.* **130**, 441–452.

Brachet, M. E., Meneguzzi, M., Vincent, A., Politano, H. & Sulem, P. L. 1992 Numerical evidence of smooth self-similar dynamics for three-dimensional ideal flows. *Phys. Fluids* **4**, 2845.

Constantin, P. 1994 Geometric statistics in turbulence. *SIAM Rev.* **36**, 73.

Constantin, P. 2000 The Euler equations and nonlocal conservative Riccati equations. *Intl Maths Res. Not.* **9**, 455–465.

Constantin, P. & Fefferman, C. 1993 Direction of vorticity and the problem of global regularity for the Navier–Stokes equations. *Indiana Univ. Maths J.* **42**, 775.

Constantin, P., Fefferman, Ch. & Majda, A. 1996 Geometric constraints on potentially singular solutions for the 3D Euler equations. *Commun. Partial Difffl Equat.* **21**, 559–571.

Grauer, R., Marliani, C. & Germaschewski, K. 1998 Adaptive mesh refinement for singular solutions of the incompressible Euler equations. *Phys. Rev. Lett.* **80**, 4177–4180.

Kerr, R. M. 1993 Evidence for a singularity in the three-dimensional Euler equations. *Phys. Fluids* **6**, 1725.

Kida, S. 1985 Three-dimensional periodic flows with high-symmetry. *J. Phys. Soc. Japan* **54** 2132.

Kida, S. & Takaoka, M. 1994 Vortex reconnection. *Ann. Rev. Fluid Mech.* **26**, 169–189.

Leray, J. 1934 Sur le mouvement d'un liquide visqueux emplissant l'space. *Acta Math.* **63**, 193–248.

Majda, A. 1986 Vorticity and the mathematical theory of incompressible fluid flow. *Commun. Pure Appl. Maths* **39**, S187–S220.

Malham, S. J. A. 2000 Collapse of a class of three-dimensional Euler vortices. *Proc. R. Soc. Lond.* A **456**, 2823–2833.

Moffatt, H. K. 2000 The interaction of skewed vortex pairs: a model for blow-up of the Navier–Stokes equations. *J. Fluid Mech.* **409**, 51–68.

Morf, R. H., Orszag, S. A. & Frisch, U. 1980 Spontaneous singularity in three-dimensional inviscid, incompressible flow. *Phys. Rev. Lett.* **44**, 572.

Necas, J., Ruzicka, M. & Sverak, V. 1996 On Leray's self-fimilar solutions of the Navier–Stokes equations. *Acta Math.* **176**, 283–294.

Neri, U. 1971 *Singular Integrals*. Springer.

Ohkitani, K. & Gibbon, J. D. 2000 Numerical study of singularity formation in a class of Euler and Navier–Stokes flows. *Phys. Fluids* **12**, 3181–3194.

Pelz, R. B. 1997 Locally self-similar, finite-time collapse in a high-symmetry vortex filament model. *Phys. Rev.* E **55**, 1617.

Pumir, A. & Siggia, E. D. 1987 Vortex dynamics and the existence of solutions to the Navier–Stokes equations. *Phys. Fluids* **30**, 1606.

Pumir, A. & Siggia, E. D. 1990 Collapsing solutions to the 3-D Euler equations. *Phys. Fluids* **2**, 220.

Shelley, M. J., Meiron, D. I. & Orszag, S. A. 1993 Dynamical aspects of vortex reconnection of perturbed anti-parallel vortex tubes. *J. Fluid Mech.* **246**, 613–652.

Siggia, E. D. 1985 Collapse and amplification of a vortex filament. *Phys. Fluids* **28**, 794.

Siggia, E. D. & Pumir, A. 1985 Incipient singularities in the Navier–Stokes equations. *Phys. Rev. Lett*. **55**, 1749.

Taylor, G. I. & Green, A. E. 1937 Mechanism of the production of small eddies from large ones. *Proc. R. Soc. Lond.* A **158**, 499.

Tsai, T.-P. 1998 On Leray's self-fimilar solutions of the Navier–Stokes equations satisfying local energy estimates. *Arch. Rat. Mech. Anal.* **143**, 29–51.

Waele, A. T. A. M. de & Aarts, R. G. K. M. 1994 Route to vortex reconnection. *Phys. Rev. Lett*. **72**, 482–485.